NANO LETTERS

Letter

pubs.acs.org/NanoLett

Terahertz Quantum Plasmonics of Nanoslot Antennas in Nonlinear Regime

Joon-Yeon Kim,[*,†] Bong Joo Kang,[*,‡] Joohyun Park,[§] Young-Mi Bahk,[†] Won Tae Kim,[‡] Jiyeah Rhie,[†] Hyeongtag Jeon,[§,∥] Fabian Rotermund,[‡] and Dai-Sik Kim[†]

[†]Department of Physics and Astronomy and Center for Atom Scale Electromagnetism, Seoul National University, Seoul 08826, Korea

[‡]Department of Physics and Department of Energy Systems Research, Ajou University, Suwon 16499, Korea

[§]Department of Nanoscale Semiconductor Engineering and [∥]Division of Materials Science and Engineering, Hanyang University, Seoul 04763, Korea

S *Supporting Information*

ABSTRACT: Quantum tunneling in plasmonic nanostructures has presented an interesting aspect of incorporating quantum mechanics into classical optics. However, the study has been limited to the subnanometer gap regime. Here, we newly extend quantum plasmonics to gap widths well over 1 nm by taking advantage of the low-frequency terahertz regime. Enhanced electric fields of up to 5 V/nm induce tunneling of electrons in different arrays of ring-shaped nanoslot antennas of gap widths from 1.5 to 10 nm, which lead to a significant nonlinear transmission decrease. These observations are consistent with theoretical calculations considering terahertz-funneling-induced electron tunneling across the gap.

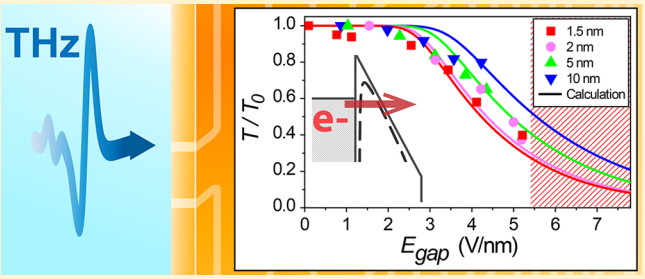

KEYWORDS: *Terahertz nonlinearity, quantum plasmonics, terahertz nanoslot antenna, metal−insulator−metal tunneling, aluminum oxide*

Plasmonic systems enter the regime of quantum mechanics as the separation between two metals becomes small enough for electrons to tunnel through the potential barrier of subnanogaps.[1,2] Experimental studies demonstrated that quantum effects on optical responses, such as charge-transfer plasmon modes, are observed at interparticle distances of around 1 nm or even less,[3−7] and an effective model has been proposed to describe those phenomena in a classical electrodynamic framework.[8] By applying a sufficiently intense electric pulse of light, however, barriers well over 1 nm are pulled down faster than the speed modern electronics can offer in the fashion of tunnel ionization in atoms and interband Zener tunneling in dielectrics.[9,10] In the long-wavelength terahertz region, the potential drop from electric fields is completely concentrated at the dielectric gap without penetration into the metal due to the high contrast of optical constant in this frequency range, enabling direct probe of nonlinear response throughout the nanogap. With lithography-based techniques that allow the fabrication of millimeter-long nanometric junctions to couple terahertz waves from free space,[11] there is an intriguing possibility of extending quantum plasmonics into the supernanometer regime and for strong fields of several volts per nanometer.

Here, we show that with terahertz transmission through vertical nanogaps, as sketched in Figure 1a, it becomes possible to initiate a nonlinear response from tunneling barriers extending beyond 1 nm. Tuning the spectra into the Hagen-Rubens regime[12] and exploiting high field enhancements as well as cross-sectional enhancements in terahertz nanoantennas[13] are all essential to reach the quantum regime from wide gaps. Within a single-cycle waveform of terahertz radiation, a transient voltage is induced across an insulating layer that significantly bends the conduction band of the dielectric toward the Fermi energy of metals (Figure 1b). Consequently, the probability for electrons to tunnel through the potential barrier dramatically increases even for thick barriers, disturbing the flow of terahertz waves in the nanogap.

To examine tunneling by an oscillating field of amplitude E_{THz}, the transient field E_{THz} must be strong enough to cause a voltage drop equal to the potential barrier height φ of interest over lengths of the order of 10 atomic distances. In addition to the development of high-power terahertz sources, especially the recent advances in table-top generation of intense terahertz pulses,[14] metallic nanogaps or antennas that enable huge field enhancements have made it possible to realize a strong enough E_{THz} near these structures.[15−17] Such intense terahertz near fields have enabled carrier multiplication through impact ionization[18,19] and ionization of ambient atoms.[20] So far, terahertz features of tunneling have been accessed from the aspects of field emission,[21−23] scanning tunneling microscopy,[24]

Received: June 24, 2015
Revised: September 6, 2015
Published: September 15, 2015

DOI: 10.1021/acs.nanolett.5b02505
Nano Lett. 2015, 15, 6683−6688

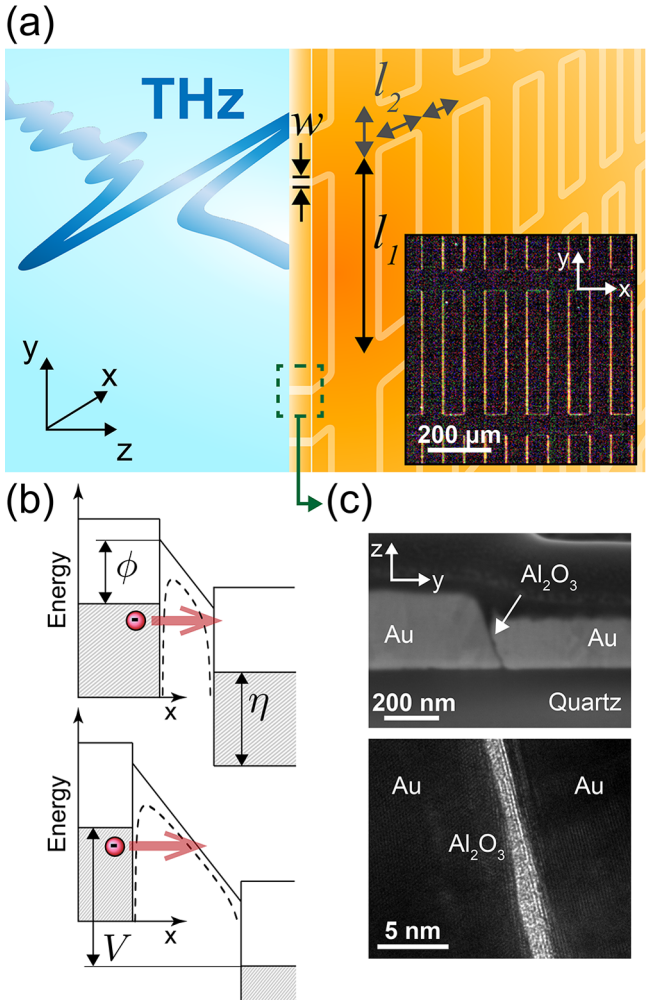

Figure 1. (a) Terahertz pulse is irradiated onto the nanogap-slot antenna structure. An optical micrograph of 10 nm gap nanoslot antennas is shown in the bottom right corner. (b) In the presence of a high electric field E_{gap}, Fermi level η in two metals separate by a potential energy of V (= $eE_{gap}w$), where φ is the barrier height defined for a rectangular barrier. Tunneling of electrons occur through barriers thick or thin. Dotted lines depict the barrier including image forces. (c) Cross-section image of a 1.5 nm wide nanogap from a scanning electron microscope (top), and a scanning transmission electron micrograph of the Al_2O_3 layer between gold (bottom).

or photon-assisted tunneling[25] and electroluminescence[26] in semiconductors. A terahertz resonant tunneling diode integrated with a slot antenna has also been investigated as a possible candidate for high-speed terahertz communications.[27] Recently, modulation of electron delocalization on the order of picoseconds has been reported,[28] where intergrain tunneling was involved. Nevertheless, a quantitative investigation on terahertz response of electron tunneling through nanogaps has been lacking because of difficulties to fabricate tunneling junctions over millimeter length scales with nanometer resolution.

We prepared nanogap-slot antennas based on atomic layer deposition (ALD) as reported previously by Chen and Park et al.[11] Gold or silver metal patterns on top of a quartz substrate are coated with aluminum oxide (Al_2O_3) using remote plasma ALD. The thickness of Al_2O_3 layer, which specifies the gap size, is controlled by the number of ALD cycles and verified by electron microscope images (Figure 1c). The minimum reliable thickness to produce the nanogaps was equal to an average of 1.5 ± 0.3 nm. Adhesive tape is used to remove excess metal to planarize the entire sample surface and reveal the ring-shaped slot antenna arrays.

High-power broadband terahertz pulses for transmission measurements are generated via pulse-front tilted optical rectification in a prism-cut lithium niobate crystal using femtosecond pulses (wavelength of 800 nm, pulse energy of 2 mJ, and pulse duration of 100 fs) from a 1 kHz Ti:sapphire regenerative amplifier. Electric field of up to 200 kV/cm is attained at the focal point in air,[29] and a pair of wire-grid polarizers is used to vary the field strength. After generation, terahertz pulses are guided by a set of off-axis parabolic mirrors and subsequently focused on a 0.3 mm thick GaP crystal or a 1 mm thick ZnTe crystal for detection by electro-optic sampling. Transmission from nanoslot antennas relative to a bare quartz substrate is measured by employing far-field terahertz time-domain spectroscopy. Derived from Kirchhoff integral formalism,[30] peak near-field enhancement is evaluated in the time domain after multiplying the peak-normalized amplitude by the ratio of total illuminated area to the total area of nanogaps excluding those sides of the ring that are aligned parallel to the electric field of the normally incident terahertz wave (see Supporting Information).

Transmitted terahertz field amplitudes are collected for the following gold or silver nanoslot antenna arrays (see Figure 1a): 1.5 nm gap (w = 1.5 nm, l_1 = 40 μm, l_2 = 10 μm), 2 nm gap (w = 2 nm, l_1 = 80 μm, l_2 = 20 μm), 5 nm gap (w = 5 nm, l_1 = 300 μm, l_2 = 50 μm), and 10 nm gap (w = 10 nm, l_1 = 300 μm, l_2 = 50 μm), which possess a resonant frequency of 0.3, 0.2, 0.1, and 0.1 THz, respectively. Different dimensions of nanoslot antennas are arranged such that the peak gap fields are closely aligned with respect to the incident power spectrum. Figure 2a presents transmitted amplitudes through a 1.5 nm gap gold nanoslot antenna for different incident peak electric field strengths. As the incident field on the nanoslot antenna surface approaches a maximum of 150 kV/cm, the transmitted field is considerably reduced. Fourier transformation of time traces displays a 35% decrease of the resonance peak at 0.3 THz in the transmitted amplitude spectrum accompanied by a slight red shift of 0.02 THz. Figure 2b shows that the temporally integrated transmittance ($T \equiv \int E^2_{sample}(t)dt / \int E^2_{reference}(t)dt$), which is normalized by the transmittance T_0 at the minimum incident field, eventually reduces by 50% as the field inside the gap E_{gap} rises to 5 V/nm. It is impractical to attain high field strengths for static fields since a maximum breakdown field of under 2−3 V/nm is expected in Al_2O_3 layers as thin as 1−1.5 nm and below 1 V/nm for layers thicker than 10 nm.[31] Moreover, field enhancements in the visible or infrared range are a few orders of magnitude lower than those at terahertz frequencies,[32] requiring higher fluence of radiation on the plasmonic structure.

Nonlinear transmission from nanoslot antennas are analyzed by considering a harmonic time dependence of the fields as depicted in the inset of Figure 2b to characterize the dielectric response ε of the gap medium at an angular frequency of ω. Assuming that the tunneling current density J causes an imbalance of electric charges nearby the metal edges through the continuity equation, the density of dipole moments or a polarization of $P = i(J/\omega)e^{-i\omega t}$ is obtained for the tunneling charges when an electric field $E = E_{gap}e^{-i\omega t}$ is present exclusively between the metals. Thus, from the relation $\varepsilon E = \varepsilon_d E + P$, the imaginary part of the dielectric quantity yields $\mathrm{Im}\{\varepsilon/\varepsilon_0\} = J/$

DOI: 10.1021/acs.nanolett.5b02505
Nano Lett. 2015, 15, 6683−6688

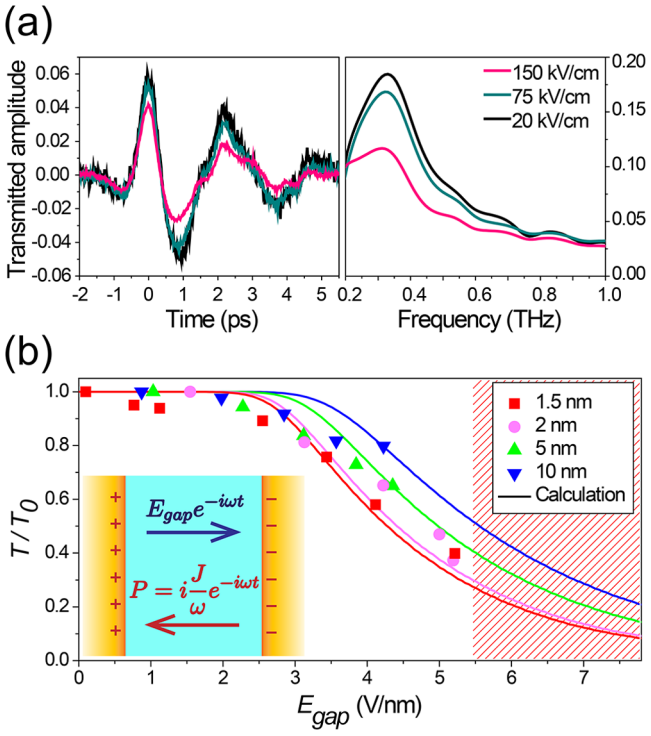

Figure 2. (a) Temporal amplitude profile (left) and the corresponding Fourier-transformed spectra (right) of terahertz waves transmitted through a 1.5 nm gap gold nanoslot antenna for different incident field strengths. (b) Terahertz transmittance as a function of electric field amplitude E_{gap} inside the nanogap for nanoslot antennas of different gap sizes. Transmission values are normalized by transmittance T_0 measured with minimum incident field strengths. Calculations are shown as solid curves. Dashed region in the right indicates that nanogaps are damaged at fields greater than 5 V/nm. Inset: Illustration of an electric field of amplitude E_{gap} oscillating at a frequency ω inducing a polarization P that is characterized by the tunneling current density J.

$\varepsilon_0\omega E_{gap}$, where ε_d is the permittivity of the gap material at zero electric field and ε_0 is the vacuum permittivity. The same expression can be derived from the quantum-corrected model[8] for interparticle separations that are not too small if J/E_{gap} is replaced by the conductivity of the plasmonic gap. Our approach in the low-frequency terahertz regime, however, simplifies the relationship connecting the classical description of ε and the quantum mechanical phenomena of tunneling by discarding the need of parameters in the Drude model pertaining to the plasma frequency or the relaxation time.

For Al_2O_3 thickness of 1.5, 2, 5, and 10 nm, the refractive index $(\varepsilon_d/\varepsilon_0)^{1/2}$ is assigned the values of 1.7, 1.75, 2.1, and 2.35 respectively.[11] Tunneling current density J is a function of gap voltage $V_{gap} = E_{gap}w$, where w is the gap width and is obtained by integrating all the electron's energy levels (see Supporting Information).[33] The effect of image forces are included to smooth out the corners of the rectangular potential barrier with a height of 3.7 eV.[34,35] With the calculated value of $\mathrm{Im}\{\varepsilon/\varepsilon_0\}$ assigned to the gap medium, field enhancement at the resonant frequency is attained by an analytical calculation of a rectangular slot antenna array based on modal expansion.[36] The monochromatic approach in part reflects the resonance in our structure, which indicates the advantage of being sensitive to local variations in charge transfers through the gap as opposed to nonresonant slit structures.[37] Dimensions of the rectangular slots for modal expansions are chosen to best resemble the actual ring-aperture-shaped nanoslot antenna array. On the basis of the Kirchhoff formalism and the simplicity of having a single frequency component, the average relative transmittance T/T_0 is evaluated reversely from the square of the ratio of field enhancement values when an applied gap field varies sinusoidally from zero to a peak value of E_{gap}. A Gaussian function is used to calculate the weighted average of the transmittance to take into account of the nonuniform field distribution across the sample area at the terahertz focus.

When strong field gradients are applied to wide gaps, the effective barrier region only accounts for a fraction of the gap (see bottom figure of Figure 1b). Specifically, it is not clear whether the overall dielectric response from the gap should be spoiled or preserved by the continuum of electrons in the conduction band of dielectrics after a Fowler–Nordheim tunneling.[38] We reduced this complicated picture by assigning the value ε to the entire volume between the metal even for wide gaps by considering the aforementioned steady-state solution of the oscillating tunneling charges. Scattering rate of electrons in the conduction band of dielectrics are known to be in the order of femtoseconds,[39,40] and therefore an equilibrium condition is reached in less than the picosecond time scale of pulse duration. The collective behavior of substantial decrease in transmission observed from barriers that are 1.5 nm thick to widths as large as 10 nm is well demonstrated in the calculations with the representation of the overall gap medium by a uniform value of ε as presented in Figure 2b. The small but meaningful resonant frequency shift of 0.02 THz is also expected from the change of the dielectric constant in the presence of tunneling. An increase in the value of $\mathrm{Im}\{\varepsilon/\varepsilon_0\}$ leads to a small increase in the real part of the index of refraction, which results in the observed red shift of the resonance.

Application of terahertz fields has the advantage of applying intense electric fields in a contactless manner using high-power pulsed radiation. By multiplying the gap width to the previously obtained transient field strength inside the gap, the gap voltage V_{gap} is derived. Because of the single-cycle nature of terahertz pulses, up to 8 V is reached across 1.5 nm gaps and 42 V across 10 nm gaps (Figure 3a). Each peak voltage has been plotted in Figure 3b for a range of incident fields for different gap sizes. Voltage across the gap increases linearly in the beginning with a gradient equal to the field enhancement times the gap width at low incident fields. On the other hand, transmission deviates from the initial linear regime as fields grow stronger. To compare with experimental results, the incident field is calculated backward by dividing E_{gap} $(= V_{gap}/w)$ by the field enhancement attained from the modal expansion calculation. Field enhancement values from measurements using low-intensity fields are used to fit the initial slope of the curves. Qualitatively, as the incident field increases, E_{gap} is enhanced or V_{gap} builds up across the gap until the peak tunneling current density $J(V_{gap})$ becomes significant enough to prevent further charge accumulation at the metal edges and brings about a reduced field enhancement. As a result, the gap voltage V_{gap} departs from the linear regime. The nonlinear field response is well displayed in Figure 3b for both calculation and experimental results.

Inasmuch as electric and magnetic fields of magnitude E_0 and H_0, which are related by the vacuum impedance Z_0 in free space, induce a surface current $\vec{K}_0 = \hat{n} \times (2\vec{H}_0)$ in perfect electric conductors, terahertz transmission measurement

DOI: 10.1021/acs.nanolett.5b02505
Nano Lett. 2015, 15, 6683−6688

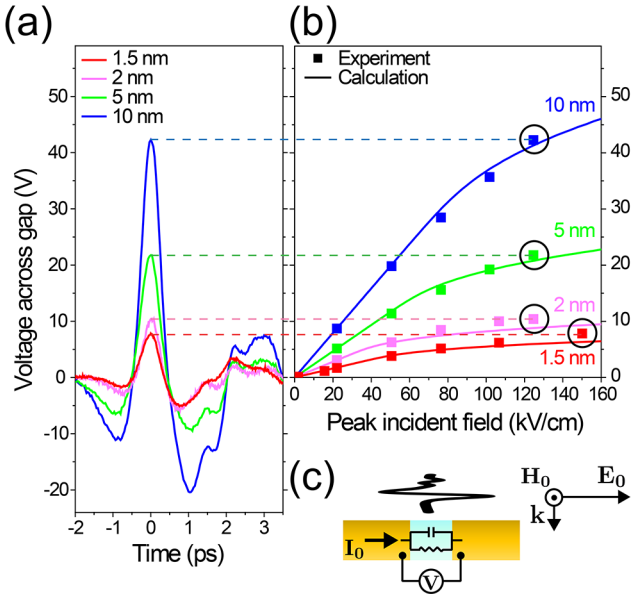

Figure 3. (a) Transmitted amplitude profile of terahertz waves for different gap widths at maximum incident field strengths. Field enhancement values and gap sizes are multiplied to estimate the voltage across gap. (b) Peak voltage across gap of 1.5, 2, 5, and 10 nm gap nanoslot antennas according to different strengths of incident field. Calculations are shown as solid curves. (c) Illustration of terahertz transmission experiment as a tunneling current−voltage measurement.

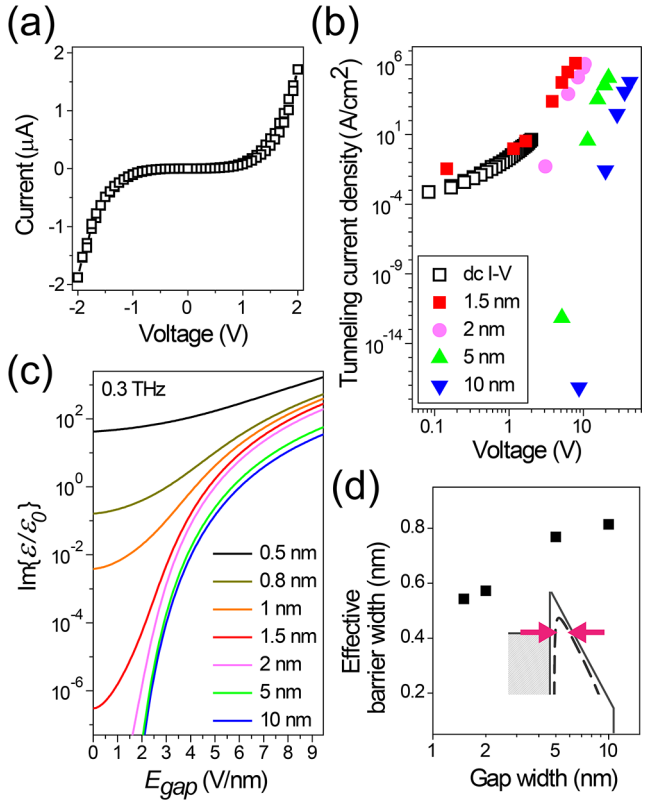

Figure 4. (a) Tunneling current measurement of a 1.5 nm gap slot antenna using two-probe dc electrical characterization. (b) Estimation of tunneling current density through different gap widths from terahertz measurement data. (c) Calculation of the imaginary part of dielectric response ε of the gap medium as a function of field amplitude inside the gap for different gap widths at 0.3 THz. (d) Calculated effective barrier width at maximum incident field strengths for different gap widths.

through nanogaps are visualized as a current−voltage measurement via an alternating current source of terahertz frequencies (Figure 3c). Hence, Figure 3b resembles a tunneling current−voltage (I−V) curve, because the incident field is proportional to the current I_0 and the transmitted field to the transient voltage V_{gap} across the gap. It is already known that nanogaps made by slits exhibit a capacitor-like behavior.[17] If the impedance Z of the slit formed between two parallel plates is described by a capacitance $C = \varepsilon_d A/w$, where A denotes the area, then by substituting the complex value ε for ε_d yields the total impedance Z^* through the relation $1/Z^* = 1/Z + 1/Z_{tunnel}$, where $Z_{tunnel} = (w/A)[1/(\mathrm{Im}\{\varepsilon/\varepsilon_0\}\varepsilon_0\omega)] = (w/A)(E_{gap}/J)$ designates the tunnel resistance of the nanogap. With intense fields, resistivity against tunneling currents appears in addition to the innate capacitance, and the total impedance connects the transient voltage to the current induced by the incident radiation.

A two-probe I−V measurement is performed on nanoslot antennas with a gap size of 1.5 nm for dc tunneling electrical characterizations as shown in Figure 4a. One of the probes is connected to the interior of the rectangular pattern while another is connected to the surrounding metal. In Figure 4b, the measured dc current is divided by the perimeter of the nanoslot antenna and by the thickness of the metal to obtain the tunneling current density. From the terahertz measurement data shown in Figure 3b, the I−V plot is acquired by matching the peak voltage across the gap with the tunneling current density value that corresponds to the peak incident field value in the calculation curve of Figure 3b. Connection between dc and terahertz measurements for a 1.5 nm gap confirms that the expression for $\mathrm{Im}\{\varepsilon/\varepsilon_0\}$ properly represents the tunneling effect at the nanogap, while also presenting terahertz measurements as an extension to electronic measurements past the dc breakdown of dielectrics.

Considering that $\mathrm{Im}\{\varepsilon/\varepsilon_0\}$ is directly proportional to the tunneling current density J from the simple model of oscillating tunneling charges, the I−V plot from terahertz measurements in combination with dc I−V measurements (Figure 4b) is fully consistent with $\mathrm{Im}\{\varepsilon/\varepsilon_0\}$ of the gap medium that is calculated as a function of field strength inside the nanogaps as is depicted in Figure 4c. Compared with subnanometer gaps, larger gap sizes suffer from a negligible $\mathrm{Im}\{\varepsilon/\varepsilon_0\}$ in unbiased conditions even with the benefits from a thousand times larger value of $\mathrm{Im}\{\varepsilon/\varepsilon_0\}$ than at visible or near-infrared frequencies. A nonzero value of $\mathrm{Im}\{\varepsilon/\varepsilon_0\} = 0.1$ is realized for the largest gap width of 10 nm when a uniform field amplitude of 5 V/nm promotes tunneling across the gap, leading to a change in the refractive index value from 2.35 to a complex value of $2.35 + 0.02i$. Within the environment of enhanced electric fields created inside the nanoslot antennas, the absorption cross section of the gap medium is enhanced to ultimately render a notable difference in transmittance which is detected through terahertz spectroscopy.[13]

Width of the potential barrier including image forces is estimated at the Fermi level for maximally biased conditions as displayed in Figure 4d. Because tunneling currents are dominated by those electrons near the Fermi surface, this width specifies an effective barrier width that the electrons encounter at the metal−dielectric interface. Transient voltage values corresponding to that circled in Figure 3b are used in the calculations for each gap width of the nanoslot antennas. An

DOI: 10.1021/acs.nanolett.5b02505
Nano Lett. 2015, 15, 6683−6688

effective barrier width of 0.5−0.8 nm is acquired from gap sizes of 1.5 to 10 nm, showing that transient terahertz fields thin the effective barrier width below a nanometer and bring about a large amount of tunneling current of 10^5−10^6 A/cm^2 as indicated in Figure 4b, regardless of its apparent thickness. The potential barrier will effectively thin to a few angstroms when field strengths become even stronger than 5 V/nm, eventually leading to a landslide of tunneling electrons through field emission,[21−23] from which nanogaps are irreversibly damaged. Wider nanogaps happen to be damaged at a slightly lower field gradient, which is thought to be related to the avalanche carrier generation process due to accelerating charges by the large applied voltage along the conduction band of aluminum oxide.

In conclusion, we have demonstrated terahertz quantum plasmonics in gap sizes of up to 10 nm using nanoslot antennas. Intense terahertz fields cause a giant nonlinear response through the nanogaps and the result is explained by considering the steady-state polarization density of tunneling electrons. Immense low-frequency fields distort and thin the nanoscale potential barrier, manipulating the effective thickness of the barrier felt by electrons into the angstrom range. Our approach of terahertz spectroscopy enlarges the boundaries of the study of quantum effects in the optical properties of plasmonic systems down to frequencies of 0.1 THz, up to field amplitudes of 5 V/nm, and barrier widths as large as 10 nm.

■ ASSOCIATED CONTENT

Supporting Information

The Supporting Information is available free of charge on the ACS Publications website at DOI: 10.1021/acs.nanolett.5b02505.

Estimation of terahertz near-field enhancement and calculation of tunneling current density. (PDF)

■ AUTHOR INFORMATION

Corresponding Authors

*E-mail: (J.-Y.K.) joonyeon@snu.ac.kr.
*E-mail: (B.J.K.) pxhwk@ajou.ac.kr.

Notes

The authors declare no competing financial interest.

■ ACKNOWLEDGMENTS

This work was supported by the National Research Foundation of Korea (NRF) grant funded by the Korea government (MSIP: NRF-2005-0093838, NRF-2015R1A3A2031768, NRF-2011-0017494, WCI 2011-001) (MOE: BK21 Plus Program-21A20131111123).

■ REFERENCES

(1) Tame, M. S.; McEnery, K. R.; Özdemir, S. K.; Lee, J.; Maier, S. A.; Kim, M. S. *Nat. Phys.* **2013**, *9*, 329−340.
(2) Zuloaga, J.; Prodan, E.; Nordlander, P. *Nano Lett.* **2009**, *9*, 887−891.
(3) Savage, K. J.; Hawkeye, M. M.; Esteban, R.; Borisov, A. G.; Aizpurua, J.; Baumberg, J. J. *Nature* **2012**, *491*, 574−577.
(4) Scholl, J. A.; García-Etxarri, A.; Koh, A. L.; Dionne, J. A. *Nano Lett.* **2013**, *13*, 564−569.
(5) Tan, S. F.; Wu, L.; Yang, J. K. W.; Bai, P.; Bosman, M.; Nijhuis, C. A. *Science* **2014**, *343*, 1496−1499.
(6) Zhu, W.; Crozier, K. B. *Nat. Commun.* **2014**, *5*, 5228.
(7) Bahk, Y.-M.; Kang, B. J.; Kim, Y. S.; Kim, J.-Y.; Kim, W. T.; Kim, T. Y.; Kang, T.; Rhie, J.; Han, S.; Park, C.-H.; Rotermund, F.; Kim, D.-S. *Phys. Rev. Lett.* **2015**, *115*, 125501.
(8) Esteban, R.; Borisov, A. G.; Nordlander, P.; Aizpurua, J. *Nat. Commun.* **2012**, *3*, 825.
(9) Corkum, P. B. *Phys. Rev. Lett.* **1993**, *71*, 1994−1997.
(10) Schiffrin, A.; Paasch-Colberg, T.; Karpowicz, N.; Apalkov, V.; Gerster, D.; Mühlbrandt, S.; Korbman, M.; Reichert, J.; Schultze, M.; Holzner, S.; Barth, J. V.; Kienberger, R.; Ernstorfer, R.; Yakovlev, V. S.; Stockman, M. I.; Krausz, F. *Nature* **2012**, *493*, 70−74.
(11) Chen, X.; Park, H.-R.; Pelton, M.; Piao, X.; Lindquist, N. C.; Im, H.; Kim, Y. J.; Ahn, J. S.; Ahn, K. J.; Park, N.; Kim, D.-S.; Oh, S.-H. *Nat. Commun.* **2013**, *4*, 2361.
(12) Dressel, M.; Grüner, G. *Electrodynamics of Solids: Optical Properties of Electrons in Matter*; Cambridge University Press: Cambridge, 2003.
(13) Park, H.-R.; Ahn, K. J.; Han, S.; Bahk, Y.-M.; Park, N.; Kim, D.-S. *Nano Lett.* **2013**, *13*, 1782−1786.
(14) Hoffmann, M. C.; Fülöp, J. A. *J. Phys. D: Appl. Phys.* **2011**, *44*, 083001.
(15) Bagiante, S.; Enderli, F.; Fabiańska, J.; Sigg, H.; Feurer, T. *Sci. Rep.* **2015**, *5*, 8051.
(16) Razzari, L.; Toma, A.; Shalaby, M.; Clerici, M.; Zaccaria, R. P.; Liberale, C.; Marras, S.; Al-Naib, I. A. I.; Das, G.; De Angelis, F.; Peccianti, M.; Falqui, A.; Ozaki, T.; Morandotti, R.; Di Fabrizio, E. *Opt. Express* **2011**, *19*, 26088−26094.
(17) Seo, M. A.; Park, H. R.; Koo, S. M.; Park, D. J.; Kang, J. H.; Suwal, O. K.; Choi, S. S.; Planken, P. C. M.; Park, G. S.; Park, N. K.; Park, Q. H.; Kim, D. S. *Nat. Photonics* **2009**, *3*, 152−156.
(18) Tarekegne, A. T.; Iwaszczuk, K.; Zalkovskij, M.; Strikwerda, A. C.; Jepsen, P. U. *New J. Phys.* **2015**, *17*, 043002.
(19) Jeong, Y.-G.; Paul, M. J.; Kim, S.-H.; Yee, K.-J.; Kim, D.-S.; Lee, Y.-S. *Appl. Phys. Lett.* **2013**, *103*, 171109.
(20) Seo, M.; Kang, J.-H.; Kim, H.-S.; Cho, J. H.; Choi, J.; Jhon, Y. M.; Lee, S.; Kim, J. H.; Lee, T.; Park, Q.-H.; Kim, C. *Sci. Rep.* **2015**, *5*, 10280.
(21) Wimmer, L.; Herink, G.; Solli, D. R.; Yalunin, S. V.; Echternkamp, K. E.; Ropers, C. *Nat. Phys.* **2014**, *10*, 432−436.
(22) Herink, G.; Wimmer, L.; Ropers, C. *New J. Phys.* **2014**, *16*, 123005.
(23) Iwaszczuk, K.; Zalkovskij, M.; Strikwerda, A. C.; Jepsen, P. U. *Optica* **2015**, *2*, 116−213.
(24) Cocker, T. L.; Jelic, V.; Gupta, M.; Molesky, S. J.; Burgess, J. A. J.; Reyes, G. D. L.; Titova, L. V.; Tsui, Y. Y.; Freeman, M. R.; Hegmann, F. A. *Nat. Photonics* **2013**, *7*, 620−625.
(25) Shibata, K.; Umeno, A.; Cha, K. M.; Hirakawa, K. *Phys. Rev. Lett.* **2012**, *109*, 077401.
(26) Lange, C.; Maag, T.; Hohenleutner, M.; Baierl, S.; Schubert, O.; Edwards, E. R. J.; Bougeard, D.; Woltersdorf, G.; Huber, R. *Phys. Rev. Lett.* **2014**, *113*, 227401.
(27) Kanaya, H.; Shibayama, H.; Sogabe, R.; Suzuki, S.; Asada, M. *Appl. Phys. Express* **2012**, *5*, 124101.
(28) Yoshioka, K.; Minami, Y.; Shudo, K.-i.; Dao, T. D.; Nagao, T.; Kitajima, M.; Takeda, J.; Katayama, I. *Nano Lett.* **2015**, *15*, 1036−1040.
(29) Baek, I. H.; Kang, B. J.; Jeong, Y. U.; Rotermund, F. *J. Opt. Soc. Korea* **2014**, *18*, 60−64.
(30) Kyoung, J. S.; Seo, M. A.; Park, H. R.; Ahn, K. J.; Kim, D. S. *Opt. Commun.* **2010**, *283*, 4907−4910.
(31) Lin, H. C.; Ye, P. D.; Wilk, G. D. *Appl. Phys. Lett.* **2005**, *87*, 182904.
(32) Ahn, J. S.; Kang, T.; Singh, D. K.; Bahk, Y.-M.; Lee, H.; Choi, S. B.; Kim, D.-S. *Opt. Express* **2015**, *23*, 4897−4907.
(33) Simmons, J. G. *J. Appl. Phys.* **1963**, *34*, 1793−1803.
(34) Afanas'ev, V. V.; Houssa, M.; Stesmans, A.; Heyns, M. M. *J. Appl. Phys.* **2002**, *91*, 3079−3084.
(35) Brewer, J. C.; Walters, R. J.; Bell, L. D.; Farmer, D. B.; Gordon, R. G.; Atwater, H. A. *Appl. Phys. Lett.* **2004**, *85*, 4133−4135.
(36) Garcia-Vidal, F. J.; Martin-Moreno, L.; Ebbesen, T. W.; Kuipers, L. *Rev. Mod. Phys.* **2010**, *82*, 729−787.

DOI: 10.1021/acs.nanolett.5b02505
Nano Lett. 2015, 15, 6683−6688

(37) Park, H.-R.; Bahk, Y.-M.; Ahn, K. J.; Park, Q. H.; Kim, D.-S.; Martín-Moreno, L.; García-Vidal, F. J.; Bravo-Abad, J. *ACS Nano* **2011**, *5*, 8340−8345.
(38) Wu, L.; Duan, H.; Bai, P.; Bosman, M.; Yang, J. K. W.; Li, E. *ACS Nano* **2013**, *7*, 707−716.
(39) Fitting, H.-J.; Hingst, Th.; Schreiber, E. *J. Phys. D: Appl. Phys.* **1999**, *32*, 1963−1970.
(40) Sun, Q.; Jiang, H.; Liu, Y.; Wu, Z.; Yang, H.; Gong, Q. *Opt. Lett.* **2005**, *30*, 320−322.

DOI: 10.1021/acs.nanolett.5b02505
Nano Lett. 2015, 15, 6683−6688